MULTISCALE MODEL. SIMUL.
Vol. 8, No. 5, pp. 1882–1901

SIMPLIFIED MODELLING OF A THERMAL BATH, WITH APPLICATION TO A FLUID VORTEX SYSTEM*

SVETLANA DUBINKINA†, JASON FRANK†, AND BEN LEIMKUHLER‡

Abstract. Based on the thermodynamic concept of a reservoir, we investigate a computational model for interaction with unresolved degrees of freedom (a thermal bath). We assume that a finite restricted system can be modelled by a generalized canonical ensemble, described by a density which is a smooth function of the energy of the restricted system. A thermostat is constructed to continuously perturb the resolved dynamics, while leaving the desired equilibrium distribution invariant. We build on a thermostatting framework developed and tested in the setting of molecular dynamics, using stochastic perturbations to control (and stabilize) the invariant measure. We also apply these techniques in the setting of a simplified point vortex flow on a disc, in which a modified Gibbs distribution (modelling a finite, rather than infinite, bath of weak vortices) provides a regularizing formulation for restricted system dynamics. Numerical experiments, effectively replacing many vortices by a few artificial degrees of freedom, are in excellent agreement with the two-scale simulations of Bühler [*Phys. Fluids*, 14 (2002), pp. 2139–2149].

Key words. thermostat methods, Nosé dynamics, Bulgac–Kusnezov, generalized canonical ensembles, point vortex fluid, unresolved dynamics

AMS subject classifications. 65M99, 65P10, 86A10, 82B99

DOI. 10.1137/100795152

1. Background.

The canonical ensemble in statistical mechanics has shown success in describing the statistical mean behavior of a system in thermal equilibrium with a large reservoir. For example, a molecular gas that is in a closed container with fixed volume and number of molecules, but is allowed to exchange kinetic energy with its surroundings, will eventually evolve to the temperature of the laboratory. Mathematically, this phenomenon is captured by the statement that the phase flow of a sufficiently complicated molecular system in contact with an infinite bath samples the Gibbs canonical distribution with density $\rho_\beta(X) = Z^{-1}\exp(-\beta H(X))$, where H is the Hamiltonian of the molecular gas in the container; β^{-1} is the statistical temperature, i.e., the average kinetic energy of the bath scaled by Boltzmann's constant; and Z is the normalization constant ensuring $\int \rho_\beta\, dX = 1$. While the canonical ensemble is certainly the most frequent choice for molecular applications, it is not the only one. The thermodynamic perspective has the potential for significant reduction of complicated models by providing a rational means for replacing a large dimensional model by one focused on a few important degrees of freedom. In this article we assume a general smooth density ρ and study extended stochastic-dynamical methods which preserve the associated phase space measure, considering an application (a vortex fluid model) with properties very different from those of molecular systems.

*Received by the editors May 12, 2010; accepted for publication (in revised form) August 20, 2010; published electronically November 16, 2010.
http://www.siam.org/journals/mms/8-5/79515.html

†Centrum Wiskunde & Informatica, P.O. Box 94079, 1090 GB Amsterdam, The Netherlands (s.dubinkina@cwi.nl, jason@cwi.nl). The first author's research was supported by the Research Council for Earth and Life Sciences (ALW) with financial aid from the Netherlands Organization for Scientific Research (NWO).

‡School of Mathematics and Maxwell Institute for Mathematical Sciences, The University of Edinburgh, James Clerk Maxwell Building, The King's Buildings, Mayfield Road, Edinburgh EH9 3JZ, Scotland (b.leimkuhler@ed.ac.uk).

In molecular dynamics, a thermostat is a tool used to model a system in thermal equilibrium; such thermostats may be either stochastic (e.g., Langevin dynamics) or deterministic. In a Langevin dynamics simulation a stochastic perturbation is introduced in the force field together with a dissipative term; these terms are maintained in balance so as to preserve the canonical ensemble. With a dynamical (or deterministic) thermostat, by contrast, the system is augmented by a few degrees of freedom that model the exchange with the reservoir. The goal of thermostatting is to force the system to sample the canonical equilibrium distribution at a given temperature by continually perturbing it. A benefit of the dynamical models is that it is possible to conserve structure (e.g., Hamiltonian structure) in the augmented dynamics. A motivation for using this approach is that if the perturbation is small, the dynamics will still correspond to physical dynamics (in contact with a reservoir) on an intermediate time scale. Some examples of important deterministic thermostatting methods are the Nosé method [19, 20], which preserves Hamiltonian structure at the expense of a continuous rescaling of time, the Nosé–Hoover method [20, 9], which recovers the linear time but loses canonical Hamiltonian structure, the Nosé–Poincaré method of Bond, Leimkuhler, and Laird [1], which is canonically Hamiltonian, and a generalization of the Nosé–Hoover approach for Hamiltonian systems with Poisson structure [3]. Deterministic thermostats have also been coupled with Langevin models in [13, 18], for example. Despite these examples, the use of thermostats as model simplifications is rarely encountered outside the molecular dynamics setting.

We are motivated in the current study by problems in inviscid fluid modelling which are natural in a number of application areas, such as atmosphere and ocean science, where the Reynolds numbers are so large as to be effectively infinite. These flows are characterized by conservation of total energy, the cascade of vorticity to ever finer scales, and sensitive dependence on initial conditions [24]. For the numerical simulation of such flows, the lack of a viscous diffusion length scale presents the challenge that, due to the vorticity cascade, any direct discretization of the equations of motion must eventually become underresolved, as vorticity is transported to scales below the grid resolution. It therefore becomes necessary to close the numerical model by some means. Any finite numerical discretization implies a closure of some kind, whether explicitly modelled or implied by the discretization [7].

The most common approach is the introduction of artificial viscosity, either through modification of the fluid equations to include (hyper-)viscosity, or through the use of stabilized discretizations, for which the viscous terms appear in a modified equation analysis [10]. In either case the viscous length scale must be on the order of the grid resolution to be effective. One disadvantage with a viscous closure model is that it precludes an upscale cascade of energy, which can be an important source of variability in geophysical flows. Alternatively, methods can be constructed that preserve the discrete total energy exactly. However, this is achieved via a nonphysical reinjection of the energy from subscale vorticity at the large scales [21].

A proper numerical closure should distinguish between resolved and unresolved dynamics and account for the exchange between these. The full complexity of dynamical interactions likely would require a more detailed treatment, such as one based on the Mori–Zwanzig formalism [5], but this would be challenging to implement flexibly, efficiently, and in generality. In this paper, as an intermediate approximation between Hamiltonian truncation and full coupled system dynamics, we describe a method to model the proper energetic exchange between resolved dynamics and thermal reservoir, under a Gibbsian partitioning assumption. We invoke a thermostat to model the unresolved vorticity and its exchange in a simple two-scale point vortex model

consisting of a small number of resolved strong vortices interacting with a very large number of unresolved weak ones. We seek a simplified computational model for the aggregate behavior of the unresolved point vortices. This situation is reminiscent of statistical mechanics in the canonical ensemble, in which a system of particles is in thermal equilibrium with a reservoir. This point of view has been exploited by Bühler [2] in a numerical/statistical investigation of the work of Onsager [22], and our goal here is to reproduce the results of [2] without explicitly accounting for the individual motions of the reservoir of weak vortices. We compare and contrast treatments based on both an infinite reservoir, as in classical thermodynamics, and a finite reservoir as has been used in the experiments of [2]. To our knowledge, this is the first systematic numerical study of the use of such an artificial thermostat reservoir, although the concept has been previously suggested [8] without essential details such as the thermostat dynamics and stochastic perturbations, and without considering finite baths or associated generalized ensembles.

The paper is structured as follows: in section 2 we make use of a generalized thermostat which can be used to force a Hamiltonian system to sample a general class of equilibrium distributions. The point vortex model and its statistical mechanics are reviewed in section 3. In section 4 we present the details of the thermostatted numerical methods considered, including the models for finite and infinite reservoirs. Finally, in section 5 the numerical schemes are verified by comparison with results from the literature.

2. Generalized thermostats. Consider an open subset $\mathcal{D} \subset \mathbb{R}^d$ and a deterministic differential equation

$$\dot{X} = f(X), \qquad X(t) \in \mathcal{D}, \qquad f : \mathcal{D} \to \mathbb{R}^d. \tag{2.1}$$

A probability distribution $\rho(X,t) \in \mathcal{D} \times \mathbb{R} \to \mathbb{R}$, $\rho \geq 0$, on $\mathcal{D}$ is transported under the vector field f according to the continuity equation

$$\frac{\partial}{\partial t}\rho(X,t) + \nabla \cdot \rho(X,t) f(X) = 0. \tag{2.2}$$

This continuity equation implies that $\int_{\mathcal{D}} \rho \, dX = 1$ for all $t > 0$ if this holds at $t = 0$. An equilibrium distribution is a stationary solution of (2.2). In this paper we will be concerned primarily with systems of the form

$$\dot{X} = J(X)\nabla H(X), \qquad X(t) \in \mathcal{D}, \quad J^T = -J, \quad H : \mathcal{D} \to \mathbb{R}. \tag{2.3}$$

The function H is a first integral of (2.3), typically the energy. If J is independent of X, then this defines a (generalized) Hamiltonian system. Otherwise, one must also show that $J(X)$ satisfies the Jacobi identity, in which case the system is Poisson. We make the weaker assumption that the vector field on the right side of (2.3) is divergence-free, i.e., $\nabla \cdot f(X) \equiv 0$, so that the transport equation (2.2) simplifies to the Liouville equation

$$\frac{d}{dt}\rho(X,t) = \frac{\partial}{\partial t}\rho(X,t) + f(X) \cdot \nabla \rho(X,t) = 0. \tag{2.4}$$

A distribution is said to be an equilibrium distribution if it is invariant under the flow (2.2), i.e., $\frac{\partial \rho}{\partial t} \equiv 0$, which in the case of (2.4) is equivalent to

$$f(X) \cdot \nabla \rho(X) \equiv 0.$$

Note that any function $\rho(X) = \rho(H(X))$ that depends on X through a first integral is an equilibrium distribution. If (2.1) has additional first integrals $I_2(X), \ldots, I_p(X)$, then any distribution $\rho(H, I_2, \ldots, I_p)$ is also an equilibrium distribution. The ensemble average of a function $F(X)$ with respect to the equilibrium distribution $\rho(X)$ is

$$\langle F \rangle := \int_{\mathcal{D}} F(X)\rho(X)\, dX.$$

Given their ample supply, the degree to which a given equilibrium distribution is meaningful largely depends on whether the solution to the differential equation is ergodic in that distribution such that the long time average of any function $F(X(t))$ of the solution

$$\overline{F} := \lim_{T\to\infty} \frac{1}{T} \int_0^T F(X(t))\, dt$$

converges to the ensemble average in the distribution, i.e., satisfies

$$\overline{F} = \langle F \rangle$$

for almost any solution trajectory. If this is the case, the equilibrium distribution characterizes the long time behavior of solutions of the differential equation.

The microcanonical ensemble [11] applies to an isolated system at constant energy and is the singular measure on the energy level set containing the initial condition

$$\rho_\mu \propto \delta(H(X) - E), \tag{2.5}$$

where $H(X(0)) = E$. This ensemble is appropriate for a numerical simulation with an energy conserving discretization.

A system in contact with a large reservoir does not conserve energy, but rather exchanges it with the reservoir. If it is in thermal equilibrium with a reservoir of statistical temperature β^{-1}, then the appropriate ensemble is the canonical ensemble [11] with Gibbs measure

$$\rho(X) = Z^{-1} \exp(-\beta H(X)), \tag{2.6}$$

where $Z = \int_{\mathcal{D}} \exp(-\beta H(X))\, dX$. It is clear, however, that a single solution of the system (2.3) will not be ergodic in the Gibbs measure, since with probability one it will sample the constant energy surface containing the initial condition, whereas (2.6) assigns nonzero probability to all energy surfaces. Instead, to model a system in thermal equilibrium with a reservoir, one must devise a method whose dynamics samples phase space with probability given by the canonical distribution (2.6). The development of methods that do just this constitutes an active field of research. A number of techniques have been developed for sampling in a given distribution, including Monte Carlo schemes, which generate random configurations or trajectories according to the chosen distribution; Langevin thermostats, in which the original system of ordinary differential equations is augmented by stochastic forcing and generalized dissipation terms; and deterministic thermostats, in which the reservoir itself is modelled using a small number of additional degrees of freedom. The latter approaches have the advantage that they generate plausible dynamics and can be used to compute correlations.

In the next two sections we describe generalized Langevin dynamics and generalized stochastic Bulgac–Kusnezov thermostats for sampling in a wide class of equilibrium distributions for Hamiltonian systems.

2.1. Langevin thermostat. If one integrates (2.3) numerically using a symplectic integrator, the Hamiltonian will be well conserved. As a result, the solution will not sample phase space with the measure (2.6) above, but instead will stay near the initial energy level set (approximately sampling ρ_μ at best). For some applications it is desirable to construct a perturbed dynamical system that does sample ρ while retaining something of the dynamical behavior of (2.3). In this way one can construct a plausible (representative) behavior of the system as if it were exchanging energy with the reservoir according to ρ.

One approach to sampling a given equilibrium distribution augments (2.3) with carefully tuned noise and dissipation terms:

$$\dot{X} = f(X) + g(X) + \Sigma(X)\dot{w}(t), \tag{2.7}$$

where $g(X) : \mathcal{D} \to \mathbb{R}^d$, $\Sigma(X) \in \mathbb{R}^{d\times d}$ is a matrix-valued function, and $w(t)$ is a vector Wiener process; i.e., the $w_i(t)$, $i = 1, \ldots, d$, are scalar Gaussian random variables with mean zero and increments $w_i(t) - w_i(s) \sim \mathcal{N}(0, t - s)$. Phase space densities are transported by the flow of (2.7) according to the Fokker–Planck equation (see, e.g., [23])

$$\frac{\partial}{\partial t}\rho(X,t) = -\nabla\cdot\rho(X,t)(f(X)+g(X)) + \frac{1}{2}\nabla\cdot\nabla\cdot\rho(X,t)\Sigma(X)\Sigma^T(X), \tag{2.8}$$

where $g(X)$ is to be determined such that the desired equilibrium distribution is a stationary solution of (2.8). If ρ depends on X only through its Hamiltonian, assuming the general form $\rho(X) = \exp F(H(X))$, then the Hamiltonian dynamics drops out of the Fokker–Planck equation, and one can solve for $g(X)$:

$$g(X) = \frac{1}{2}\nabla\cdot\Sigma\Sigma^T + \frac{1}{2}F'(H)\Sigma\Sigma^T\nabla H(X). \tag{2.9}$$

For the case of additive noise, $\Sigma = const.$, the Langevin dynamics is

$$\dot{X} = J\nabla H(X) + \frac{1}{2}F'(H)\Sigma\Sigma^T\nabla H(X) + \Sigma\dot{w}. \tag{2.10}$$

If Σ is positive definite, then the flow map is ergodic with respect to ρ, and the generalized Langevin dynamics (2.7) can be used to sample the canonical distribution at inverse temperature β, taking $F'(H) = -\beta$.

2.2. A generalized Bulgac–Kusnezov method. The following approach generalizes the Bulgac–Kusnezov method [3] and offers additional flexibility. The method has been proposed for canonical sampling in the molecular dynamics setting in [12]; here we treat an arbitrary smooth ensemble and apply it to the fluid vortex model. We introduce a new variable $\zeta \in \mathbb{R}$ and functions $s(X,\zeta) : \mathcal{D}\times\mathbb{R} \to \mathbb{R}^d$ and $h(X,\zeta) : \mathcal{D}\times\mathbb{R}\to\mathbb{R}$ and form the coupled system

$$\dot{X} = J\nabla H(X) + s(X,\zeta), \tag{2.11}$$

$$\dot{\zeta} = h(X,\zeta). \tag{2.12}$$

We ask that the following extended measure be invariant under the Liouville equation:

$$\tilde{\rho}(X,\zeta) \propto \exp(-\beta F(X) - \alpha G(\zeta)) \tag{2.13}$$

for F and G appropriately defined functions. In the case of (2.6) we will take $F \equiv H$, but we consider this more general formulation for now. Note that in this measure,

X and ζ are independent, and after integration over ζ, the measure is of the form (2.6). The stationarity condition for the transport equation (2.2) is

$$\nabla \cdot \tilde{\rho}\,(f+s) + \partial_\zeta(\tilde{\rho}h) = 0 \quad \text{with } f = J\nabla H(X).$$

Some calculations give

$$\begin{aligned} 0 &= (f+s)\cdot\nabla\tilde{\rho} + \tilde{\rho}\nabla\cdot(f+s) + h\frac{\partial}{\partial\zeta}\tilde{\rho} + \tilde{\rho}\frac{\partial}{\partial\zeta}h \\ &= -\beta\tilde{\rho}\nabla F\cdot(f+s) + \tilde{\rho}\nabla\cdot(f+s) - \alpha\tilde{\rho}h\frac{\partial}{\partial\zeta}G + \tilde{\rho}\frac{\partial}{\partial\zeta}h \\ &= \tilde{\rho}\left(-\beta\nabla F\cdot(f+s) + \nabla\cdot s - \alpha h\frac{\partial}{\partial\zeta}G + \frac{\partial}{\partial\zeta}h\right), \end{aligned}$$

where the divergence-freedom of the Hamiltonian vector field is used in the last inequality.

Next we make some simplifying assumptions. First we assume the thermostat variable ζ to be normally distributed, taking $G(\zeta) = \zeta^2/2$. We also assume that h depends only on X; i.e., $h(X,\zeta) = h(X)$. The stationarity condition consequently reduces to

$$0 = -\beta\nabla F\cdot(f+s) + \nabla\cdot s - \alpha h\zeta.$$

We wish to use this relation to define h. Note that

$$\zeta h(X) = \frac{1}{\alpha}\left(\nabla\cdot s - \beta\nabla F\cdot(f+s)\right). \tag{2.14}$$

Since ζ may be zero, each term on the right should either vanish or have precisely a factor ζ as on the left. Candidate equilibrium distributions for (2.3) typically have functional dependence via the Hamiltonian. If we assume $F(X) := F(H(X))$, then the skew-symmetry of J implies

$$\nabla F\cdot f = F'(H(X))\nabla H\cdot J\nabla H \equiv 0.$$

If additionally we assume $s(X,\zeta)$ to be linear in ζ, i.e.,

$$s(X,\zeta) = s_1(X)\zeta, \qquad s_1(X)\in\mathbb{R}^d,$$

then we find that

$$h(X) = \frac{1}{\alpha}\left(\nabla\cdot s_1(X) - \beta\nabla F\cdot s_1(X)\right) \tag{2.15}$$

is a solution of (2.14).

Specific choices of the functions $F(X)$ and $s_1(X)$ will be treated in section 4.

In general, the thermostatted dynamics so defined will not be ergodic in the invariant measure (2.13). To improve ergodicity, a Langevin term may be added to (2.12); see also [13]. That is,

$$\dot{X} = J\nabla H(X) + s_1(X)\zeta, \tag{2.16}$$

$$\dot{\zeta} = h(X) - \frac{\alpha\sigma^2}{2}\zeta + \sigma\dot{w}. \tag{2.17}$$

Since the noise enters through ζ, it influences $X(t)$ only after integration, so its effect on the dynamics is smoothed.

Remark. Proving ergodicity of (2.16)–(2.17) would require a Hörmander-type controllability analysis [17, 13]; we do not provide this here but are currently considering this challenge in separate work.

Remark. In the important special case $F(X) := F(H(X))$, if we choose s_1 such that $\nabla \cdot s_1 \equiv 0$, then the system (2.16)–(2.17) can be cast in the form of a generalized Langevin thermostat (2.10) with degenerate noise. Define the augmented system

(2.18)
$$\tilde{X} = \begin{pmatrix} X \\ \zeta \end{pmatrix}, \qquad \tilde{J}(\tilde{X}) = \begin{bmatrix} \frac{1}{F_H} J & \frac{\beta}{\alpha} s_1(X) \\ -\frac{\beta}{\alpha} s_1(X)^T & 0 \end{bmatrix}, \qquad \tilde{H}(X,\zeta) = F(H(X)) + \frac{\alpha}{2\beta}\zeta^2.$$

Then (2.16)–(2.17) with (2.15) takes the form

$$\frac{d}{dt}\tilde{X} = \tilde{J}\nabla\tilde{H} - \frac{\alpha}{2}\Sigma\Sigma^T\nabla\tilde{H}(\tilde{X}) + \Sigma\dot{w} \tag{2.19}$$

with $\Sigma = \left[\begin{smallmatrix} 0 \\ \sigma \end{smallmatrix}\right]$.

3. Statistical mechanics of point vortices. In this paper we will validate the method (2.16)–(2.17) for the classical flow of singular point vortices on a disc. The point vortex model has often been used as a simple prototype for geophysical flows, despite its numerous shortcomings [16, 15]. Proof of the weak convergence of the point vortex model as a numerical discretization is contained in the monograph [6], which also describes modern point vortex methods making use of regularized kernels and fast force evaluations and techniques for modelling 3D and viscous flows. Other references on point vortex methods are [4, 14]. Our primary motivation for using the simple model with singular point vortices is the work of [2], as it contains detailed numerical experiments and thus provides an opportunity for direct comparison.

The motion of N singular point vortices with circulation strengths $\Gamma_i \in \mathbb{R}$, $i = 1, \ldots, N$, and positions $x_i(t) \in \mathbb{R}^2$ is given by the Hamiltonian system

$$\Gamma_i \dot{x}_i = K\frac{\partial H}{\partial x_i}, \qquad i = 1, \ldots, N, \tag{3.1}$$

where $K = \left(\begin{smallmatrix} 0 & 1 \\ -1 & 0 \end{smallmatrix}\right)$, and the Hamiltonian

$$H = -\frac{1}{4\pi}\sum_{i<j}\Gamma_i\Gamma_j \ln(|x_i - x_j|^2)$$

represents the kinetic energy.

For a mixed system of both positive and negative circulations Γ_i, the motion of point vortices is unbounded on the plane. A bounded flow can be ensured by imposing periodicity, which alters the Green's function in the Hamiltonian [25]. Alternatively, flow on a disc of radius R can be modelled by defining a set of image vortices

$$\Gamma_i' = -\Gamma_i, \quad x_i' = x_i\frac{R^2}{|x_i|^2}, \quad i = 1, \ldots, N,$$

which ensure that the velocity field induced by any point vortex and its image is tangent to the wall at its intersection with the dipole axis. In the disc model, which we adopt in this paper, the Hamiltonian has three terms due to the original pair potential,

the self-interaction, and the interaction terms of each vortex with the images of the others:

$$H = -\frac{1}{4\pi}\sum_{i<j}\Gamma_i\Gamma_j \ln(|x_i - x_j|^2) + \frac{1}{4\pi}\sum_i \Gamma_i^2 \ln(R^2 - |x_i|^2) + \frac{1}{4\pi}\sum_{i<j}\Gamma_i\Gamma_j \ln(R^4 - 2R^2 x_i \cdot x_j + |x_i|^2|x_j|^2). \tag{3.2}$$

To cast the system (3.1) in the form (2.3), we define $X = (x_1^T, \ldots, x_N^T)^T$, $H = H(X)$, and

$$J = \begin{bmatrix} \Gamma_1^{-1}K & & \\ & \ddots & \\ & & \Gamma_N^{-1}K \end{bmatrix}.$$

Besides the kinetic energy, the point vortex flow on the disc conserves the total angular momentum, defined as

$$M = \frac{1}{2\pi}\sum_i \Gamma_i |x_i|^2. \tag{3.3}$$

In general there will be an exchange of momentum between the strong vortices and the reservoir. However, on average we would expect the angular momentum of both strong and weak vortex sets to be approximately constant. In fact, it would be straightforward to model the exchange of angular momentum using the thermostat as well. This would require knowledge of the variance of the angular momentum of the reservoir. In this paper we assume that the momentum exchange with the reservoir is negligible, and we can show that M is a conserved quantity of the thermostatted dynamics. Experiments with Langevin dynamics indicate significant drift in angular momentum. To correct this, one could construct a projection of the noise term $\Sigma(X)$ onto the angular momentum manifold. However, this makes the noise multiplicative, and one must include the additional term $\nabla \cdot \Sigma\Sigma^T$ of (2.9) in the Langevin dynamics (2.10).

As noted by Onsager [22], the phase space of the point vortex flow consists of the direct product of N copies of the domain. If the domain is bounded, so is the phase space. The energy H is unbounded on the phase space, however: as $x_i \to x_j$, the logarithm tends to $-\infty$; if Γ_i and Γ_j are like-signed, $H \to +\infty$, and if they are opposite-signed, $H \to -\infty$. In particular, if a point vortex collides with the wall, $H \to -\infty$. If we define $\Omega(E)$ to be the measure of the set of configurations in phase space for which $H \in (E, E + dE)$, then we must have $\lim_{E\to\pm\infty}\Omega(E) = 0$. In other words, since the phase space is bounded, the measure of available phase space must eventually decrease as a function of increasing energy. The situation is in contrast to classical n-body problems encountered in chemistry and astronomy, where the positive definite kinetic energy terms can accommodate any amount of energy and the measure of available phase space is a monotone increasing function of energy.

Consequently, the microcanonical entropy $S(E) = \ln\Omega(E)$ must attain a maximum for some E^*. The microcanonical inverse temperature is defined to be $\beta_\mu = \frac{d}{dE}\ln S(E)$, and negative temperature states occur for $E > E^*$. For a homogeneous system with $\Gamma_i = \Gamma$, the energy largely governs the dynamics, since collisions have to occur roughly at constant energy. As pointed out in [2], the situation is more

interesting in a heterogeneous system with vortices of greatly differing strength. Onsager predicted that for such systems, extreme values of energy would increase the likelihood of clustering of like-signed or opposite-signed vortices, with a preference for the strongest ones, such that most of the energy would reside in a few degrees of freedom. As a result, the small vortices would roam aimlessly about, not developing into coherent structures but contributing to large entropy.

Bühler [2] discusses Onsager's ideas in the context of the canonical ensemble applied to the strong vortices, which constitute a system in "thermal" equilibrium with the reservoir of weak vortices. In the simplest case, canonical statistical mechanics assumes a system with Hamiltonian $H(X) = H_A(X_A) + H_B(X_B)$, where X_A represents the state of the subsystem of interest and X_B represents the state of the reservoir. The dimension of X_B is assumed large. The phase space measures are denoted $\Omega_A(E_A) = \{X_A \mid H_A(X_A) = E_A\}$ and $\Omega_B(E_B) = \{X_B \mid H_B(X_B) = E_B\}$ with corresponding entropies $S_A = \ln \Omega_A$, $S_B = \ln \Omega_B$ and total entropy $S = S_A + S_B$. The probability of observing system A in state X_A, given total energy E, is

$$\begin{aligned} \text{prob}(X_A \mid H(X) = E) &\propto \Omega_B(E - E_A) \\ &= \exp\left(S_B(E - E_A)\right) \\ &= \exp\left(S_B(E) - S_B'(E)E_A + \frac{1}{2}S_B''(E)E_A^2 + \cdots\right) \\ &\propto \exp\left(-S_B'(E)E_A + \frac{1}{2}S_B''(E)E_A^2 + \cdots\right), \end{aligned} \tag{3.4}$$

where $\beta = S_B'(E)$ is the inverse temperature of the reservoir and a constant term has been absorbed into the proportionality constant. Use of the Taylor series assumes small changes in reservoir entropy over the range of subsystem energy E_A. Truncating (3.4) motivates the definition of the canonical ensemble for subsystem A,

$$\rho(X_A) \propto \exp\left(-\beta H_A(X_A)\right),$$

which is equivalent to (2.6).

In [2] Onsager's predictions are verified using numerical experiments with a system of 100 point vortices, four having strength $\pm 10\pi$ and the rest having strength $\pm 2\pi$. In each group, half the vortices had positive circulation and half negative. Simulations were done for extreme positive, neutral, and extreme negative inverse statistical temperatures β_μ in the microcanonical sense. In each case the strong vortices had the same (nearly steady state) initial configuration, so the differences in energy were due only to the random placement of weak vortices. Simulations were run on a long time interval, and statistics were recorded for the distance between like- and opposite-signed strong vortices, distance from the wall, and energy partition in the strong vortices.

The distinction is made between a theoretical infinite reservoir and the finite reservoir composed of the 96 weak vortices. In the infinite reservoir case, the canonical probability measure can be normalized only for a finite interval of inverse temperature $\beta \in (\beta^-, \beta^+)$. For reservoir temperatures outside this range, the subsystem dumps or absorbs an infinite amount of energy and collisions occur internally or with the boundary. This situation is due to the availability of an infinite amount of energy in the reservoir and has implications for thermostatting in the canonical ensemble. Contact with a finite reservoir will suppress this collapse, allowing thermostatting at all temperatures [2]. This is because there is a finite amount of energy in the

finite reservoir, and this effectively bounds the closeness of the approach of any two vortices from below, making the probability of a close approach very small. Under the assumption that the reservoir energy levels are approximately normally distributed with variance σ_B^2, a subsystem in contact with a finite reservoir has probability [2]

$$\rho(X_A) \propto \exp\left(\frac{EE_A}{\sigma_B^2} - \frac{E_A^2}{2\sigma_B^2}\right). \tag{3.5}$$

As E_A becomes large in magnitude, the second term dominates and the probability density decays relative to the canonical ensemble density at a rate proportional to $\exp(-\gamma E_A^2)$.

4. A thermostatted integrator for point vortices. Our goal is to apply the generalized Bulgac–Kusnezov thermostat from section 2.2 to the point vortex flow of section 3. In this section we fill in the details of the method. First, in section 4.1 we specify two equilibrium distributions corresponding to the cases where the reservoir of unresolved weak vortices is finite or infinite. In section 4.2 we define a thermostat function s_1 such that the generalized Bulgac–Kusnezov thermostat is a Langevin thermostat. We describe in section 4.3 the numerical method used to integrate the model adaptively in time and in section 4.4 the means of computing the temperature.

4.1. Infinite and finite reservoir ensembles. As discussed in [2] the behavior of a thermostatted point vortex system can vary considerably depending on whether the reservoir is finite or infinite. In the case of an infinite reservoir, as the temperature of the reservoir is pushed toward zero, the subsystem may draw an arbitrarily large amount of energy from the reservoir, leading to collisions between individual vortices or with the wall. For a finite reservoir, there is a limited amount of energy available such that a collision may occur only if a collision with opposite energy occurs at the same time, and this is improbable. Specifically, in the case of a finite reservoir with normally distributed reservoir energy, the equilibrium distribution takes the form

$$\tilde{\rho}(X) = \exp\left(-\beta H(X) - \gamma H(X)^2\right).$$

For the generalized thermostat (2.11)–(2.12) we can model both finite and infinite reservoirs. For a finite reservoir we take

$$F(X) := H(X) + \frac{\gamma}{\beta}H(X)^2, \qquad h(X) = \frac{1}{\alpha}\left(\nabla \cdot s_1(X) - (\beta + 2\gamma H(X))\nabla H \cdot s_1(X)\right), \tag{4.1}$$

where by comparison with (3.5), we choose $\gamma = -\beta/(2E)$. For an infinite reservoir, $\gamma \equiv 0$ in the expressions above.

4.2. Choice of s_1. We make the following choice for the function s_1 in (2.15):

$$s_1(X) = -\begin{pmatrix} \frac{Kx_1}{|x_1|} \\ \vdots \\ \frac{Kx_N}{|x_N|} \end{pmatrix}. \tag{4.2}$$

The motivation for this choice is threefold: first, the flow of the vector field s_1 preserves the distance of each point vortex from the center of the domain. Consequently, the thermostatted system (2.16)–(2.17) *preserves the angular momentum* (3.3). Second, this choice of s_1 is divergence-free:

$$\nabla \cdot s_1(X) \equiv 0,$$

implying that the thermostatted dynamics is a generalized Langevin system (2.19) and that the integral $\tilde{H}$ in (2.18) with $F(H(X))$ from (4.1) is preserved in the limit $\sigma \to 0$ of zero noise and dissipation. Third, this choice makes the magnitude of s_1 isotropic on the domain.

On the other hand, the vector field (4.2) is discontinuous for any point vortex at the origin. We observed no adverse effects of this discontinuity in our experiments, however.

4.3. Implementation details. In our numerical implementation, time stepping is done using a second order, symmetric splitting approach. We solve alternately the deterministic thermostat system and the noise-dissipation flow for the thermostat variable.

The latter flow is an Ornstein–Uhlenbeck equation,

$$\dot{\zeta} = -\frac{\alpha\sigma^2}{2}\zeta + \sigma\dot{w},$$

which for a given realization of the Wiener process $w(t)$ has exact solution

$$\zeta^{n+1} = e^{-\varepsilon\tau}\left(\zeta^n + \sigma\sqrt{\frac{e^{2\varepsilon\tau}-1}{2\varepsilon}}\Delta w\right), \tag{4.3}$$

where $\varepsilon = \alpha\sigma^2/2$ and $\Delta w \sim \mathcal{N}(0,1)$.

A full time step of size Δt is constructed by solving (4.3) with $\tau = \Delta t/2$, composed with an implicit midpoint step of size Δt for the Hamiltonian part of the vector field, composed with a second solution of (4.3), $\tau = \Delta t/2$; i.e.,

$$\zeta_0^* = e^{-\varepsilon\Delta t/2}\left(\zeta^n + \sigma\sqrt{\frac{e^{2\varepsilon\Delta t/2}-1}{2\varepsilon}}\Delta w\right), \tag{4.4}$$

$$\frac{X^{n+1}-X^n}{\tau} = J\nabla H(\hat{X}) - s_1(\hat{X})\hat{\zeta}, \tag{4.5}$$

$$\frac{\zeta_1^*-\zeta_0^*}{\tau} = h(\hat{X}), \tag{4.6}$$

$$\zeta^{n+1} = e^{-\varepsilon\Delta t/2}\left(\zeta_1^* + \sigma\sqrt{\frac{e^{2\varepsilon\Delta t/2}-1}{2\varepsilon}}\Delta w\right), \tag{4.7}$$

where $\hat{X} = (X^{n+1}+X^n)/2$ and $\hat{\zeta} = (\zeta_1^*+\zeta_0^*)/2$. Equations (4.5)–(4.6) are solved implicitly using fixed point iteration to a relative tolerance of 10^{-14}.

During a close approach of two vortices, equivalently when the strong vortex energy is large in magnitude, accuracy and stability considerations motivate the use of an adaptive time-stepping strategy. Given a step size Δt_n in the nth time step, the subsequent time step is found by solving

$$\Delta t_n \Delta t_{n+1} = \ell(X^n)^2\Delta s^2. \tag{4.8}$$

Here, Δs is a uniform time step under the time transformation $t = \ell \cdot s$, and ℓ is a monitor function that measures the stiffness of the local solution. This adaptivity approach is explicit and time-reversible whenever the numerical integrator is symmetric. For our experiments we use

$$\ell(x) = \min_{i\neq j}|x_i - x_j|,$$

where the minimization is over all vortices and image vortices.

4.4. Computation of temperatures. We check the inverse temperature β numerically assuming ergodicity. For some function $a(X) : \mathcal{D} \to \mathbb{R}^d$ and an equilibrium distribution $\rho(X) = \exp\left(-\beta^* \tilde{H}(X)\right)$,

$$\nabla \cdot \rho(X)a(X) = a(X) \cdot \nabla\rho(X) + \rho(X)\nabla \cdot a(X) = -\beta^* \rho(X)a(X) \cdot \nabla\tilde{H} + \rho(X)\nabla \cdot a(X).$$

Formally integrating over phase space,

$$\int_{\mathcal{D}} \nabla \cdot \rho(X)a(X)\, dX = -\beta^* \int_{\mathcal{D}} \rho(X)a(X) \cdot \nabla\tilde{H}\, dX + \int_{\mathcal{D}} \rho(X)\nabla \cdot a(X)\, dX. \tag{4.9}$$

The expression on the left is zero if either ρ or a is zero on the boundary $\partial\mathcal{D}$ of phase space. The boundary of $\mathcal{D}$ consists of configurations for which at least one point vortex is located on the boundary of the disc. Such a configuration has energy $H \to -\infty$. Likewise, there are points in phase space where two or more point vortices collide and the Hamiltonian tends to $\pm\infty$. The Gibbs distribution (2.6) can be normalized only for β on an open interval [2]:

$$\beta \in \left(\frac{-8\pi}{\Gamma^2 N}, \frac{+4\pi}{\Gamma^2}\right). \tag{4.10}$$

To carry out the integration (4.9), we choose a of the form

$$a = b/\rho, \qquad \rho(X) = \exp\left(-\beta H(X)\right),$$

where β is the desired inverse temperature and $b(X)$ is some function with $b = 0$ at the boundary of the phase space. In this case, the expression for β^* simplifies to

$$0 = -\beta^* \langle a \cdot \nabla\tilde{H}\rangle + \langle \nabla \cdot a\rangle.$$

If the flow is ergodic, then the ensemble averages can be replaced with time averages

$$\beta^* = \overline{\nabla \cdot a}/\overline{a \cdot \nabla\tilde{H}}, \tag{4.11}$$

and the disagreement of β^* and β serves as a simple check for nonergodicity. For the infinite reservoir, $\tilde{H} = H$, and for the finite reservoir, $\tilde{H} = H + \gamma^*/\beta^* H^2$, yielding

$$0 = -\beta^* \langle a \cdot \nabla H\rangle - 2\gamma^* \langle a \cdot H\nabla H\rangle + \langle \nabla \cdot a\rangle. \tag{4.12}$$

Choosing two independent functions $a_1 = b_1/\rho$ and $a_2 = b_2/\rho$, where b_1 and b_2 are identically zero on $\partial\mathcal{D}$, these equations yield a linear system for β^* and γ^*. In numerical simulations we observed that the averages were slow to converge for the coefficient matrix. Instead we include here only the convergence of the inverse temperature β^*, which in the finite reservoir case is computed from (4.12) by taking $\gamma^* = -\beta^*/(2E_0)$. As a monitor function we used

$$b = \nabla H \prod_i \left(1 - \frac{|x_i|^2}{R^2}\right), \quad \rho = \exp(-\beta H - \gamma H^2),$$

where β is one of the three inverse temperatures (5.1) and γ is either 0 for the infinite reservoir or the corresponding reservoir variance (5.2) for the finite reservoir.

Figure 1 illustrates convergence of β^* to the values of β (5.1) for both the infinite and finite reservoir. The parameters are taken as in section 5, except that the initial condition was perturbed, i.e., $x_1(0) = (2.9, 0.1)$, and the time averages in (4.12) were started from $T_0 = 500$.

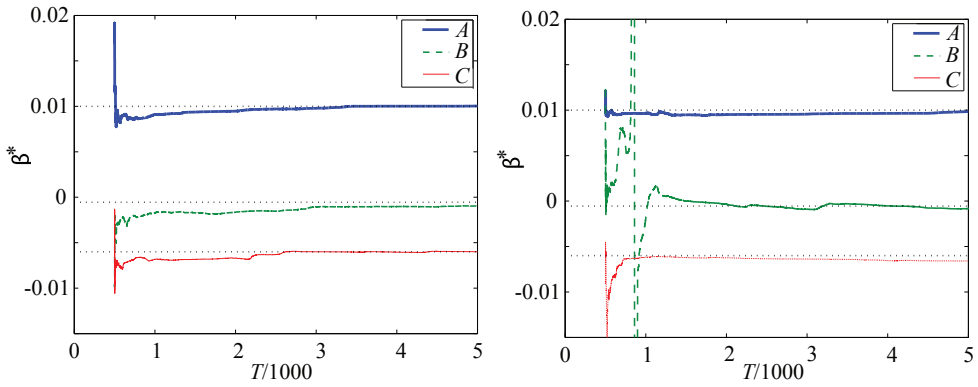

FIG. 1. *Convergence of inverse temperature approximation β^* for positive (A), neutral (B), and negative (C) inverse temperature states. Left: Infinite reservoir formula* (4.11). *Right: Finite reservoir formula* (4.12). *The dotted lines show the input values of inverse temperature β.*

5. Numerical experiments. For all of the numerical experiments using four strong vortices, the initial configuration consists of point vortices with circulations and positions given by [2]:

$$\Gamma_1 = \Gamma_3 = 10\pi, \qquad \Gamma_2 = \Gamma_4 = -10\pi,$$
$$x_1 = (3,0), \quad x_3 = (-3,0), \quad x_2 = (0,3), \quad x_4 = (0,-3).$$

For both the finite and infinite reservoir thermostats we choose negative, neutral, and positive inverse temperatures $\beta = S'_B(E)$ by estimating the slope of the graph [2, Figure 3(a)] at the desired total energies E_0, and then tuning the values to obtain a close fit to the results reported in [2]. We use

$$\beta = \{-0.006, -0.00055, 0.01\}. \tag{5.1}$$

This choice of β is close to the theoretical upper and lower limits in (4.10).

The variance of the reservoir is controlled by γ. In the case of an infinite reservoir $\gamma \equiv 0$; for a finite reservoir, from (3.5),

$$\gamma = \beta/(-2E_0), \tag{5.2}$$

where E_0 is the total energy of the resolved dynamics plus reservoir. From [2] we take $E_0 = \{628, 221, -197\}$.

As can be deduced from the invariant distribution (2.13), the parameter α controls the variability of the thermostat variable ζ and the rate at which the resolved dynamics is thermostatted. The parameter σ controls the rate of thermalization of ζ in (2.17). In all experiments we take $\alpha = 0.5$ and $\sigma = \sqrt{0.4}$.

We integrated the thermostatted dynamics over the interval $t \in [0, T]$ with $T = 12000$ using the time transformation (4.8) and fixed transformed time steps $\Delta s = \Delta t_0/\ell(X^0)$ with $\Delta t_0 = 0.001$. The sampling was performed over the time interval $[T_0, T]$ with $T_0 = 1500$ to allow decorrelation of the initial conditions. The resulting time series was sampled uniformly in time in cycles of $\delta t = 0.01$ to produce the histograms shown in Figures 6–9.

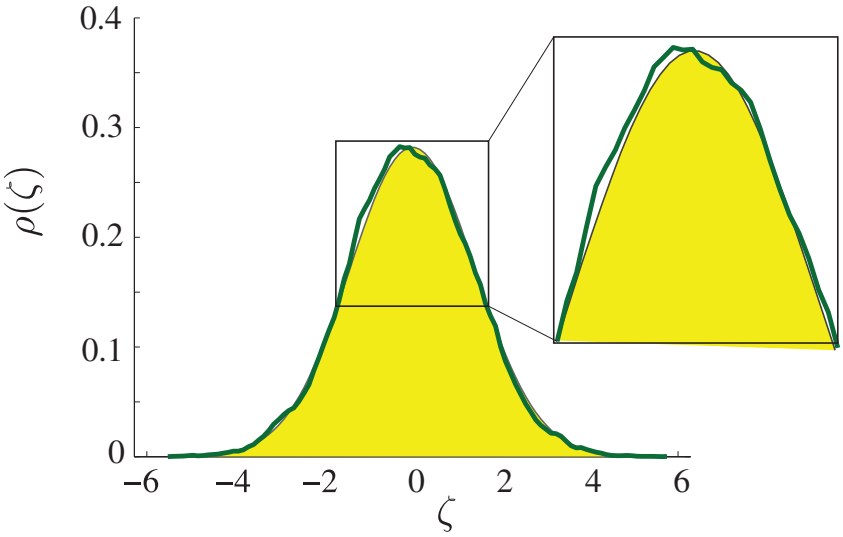

FIG. 2. *Distribution of thermostat (thick line), Gaussian fit (shaded).*

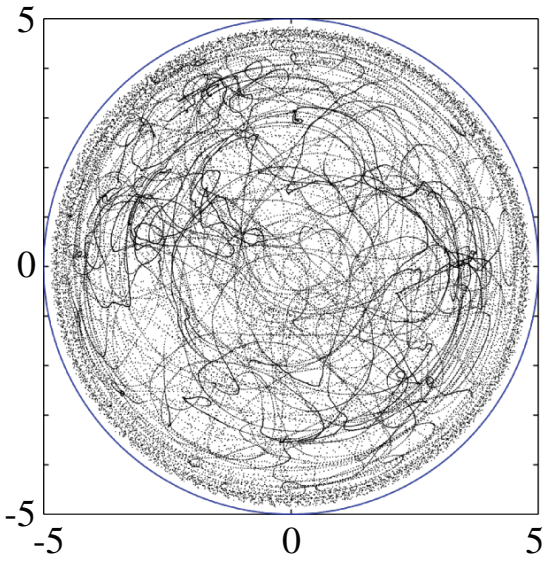

FIG. 3. *Motion of a single vortex* $x_1(t)$ *on the interval* $t \in [0, 1000]$ *for* $\beta = -0.00055$.

5.1. Ergodicity tests. The extended measure (2.13) is Gaussian in the thermostat variable ζ. If the time dynamics is ergodic with respect to (2.13), we expect the time series $\zeta(t)$ to be normally distributed; i.e., $\zeta \in \mathcal{N}(0, \alpha^{-1})$. A histogram of the values of ζ is shown in Figure 2 for the neutral case $\beta = -0.00055$. The normal distribution $\rho(\zeta) = \sqrt{\frac{\alpha}{2\pi}} \exp(-\frac{\alpha}{2}\zeta^2)$ is also plotted in the figure. The agreement is good, suggesting ergodicity with respect to ζ.

As a second indication of ergodicity, we plot the trajectory of a single vortex $x_1(t)$ in Figure 3. The motion appears well mixed. The density of points along the trajectory is greater where either the local velocity $\dot{x}_1$ or the local time step Δt_n is small.

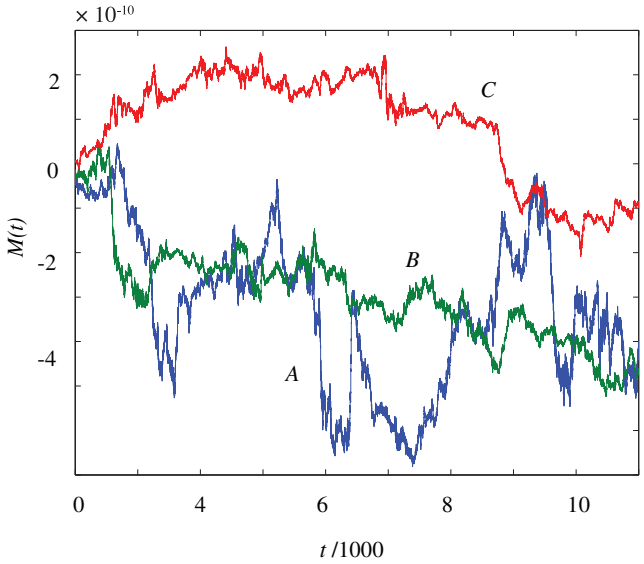

FIG. 4. *Momentum for positive (A), neutral (B), and negative (C) inverse temperature states for finite reservoir size. An infinite reservoir gives a similar behavior.*

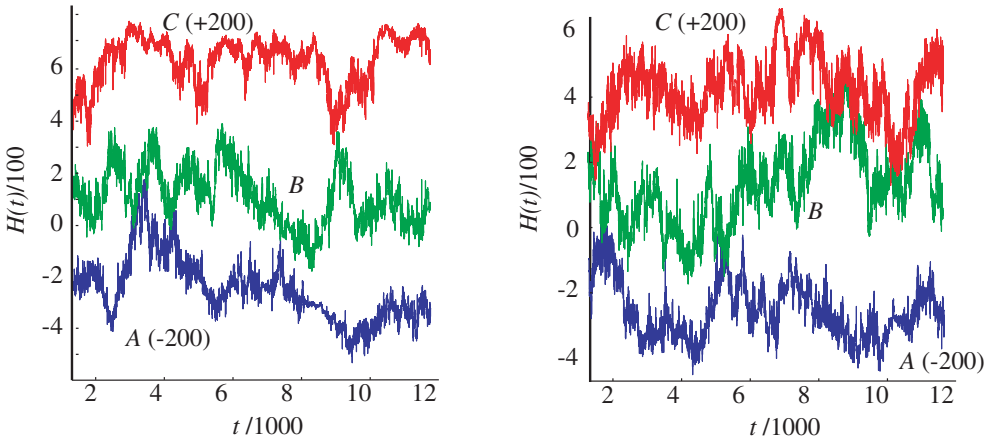

FIG. 5. *Time evolution of energy $H(t)$ for infinite (left) and finite (right) reservoirs. Inverse temperatures: $\beta = 0.01$ (A, shifted by -200), $\beta = -0.00055$ (B), $\beta = -0.006$ (C, shifted by $+200$).*

5.2. Momentum conservation. The function $s_1(X)$ in (4.2) is chosen to preserve angular momentum (3.3) of the strong vortex set under the thermostatted dynamics. Figure 4 shows the angular momentum M as a function of time for the three temperatures. We observe that M is preserved to the relative precision of the fixed point iteration used to solve (4.5)–(4.6).

5.3. Temperature effects. In this section we attempt to reproduce the experiments of Bühler using thermostatted large point vortices. We conduct experiments using both the infinite reservoir canonical distribution ((4.1) with $\gamma \equiv 0$) and the finite reservoir distribution ((4.1) with $\gamma \neq 0$).

The time evolution of the kinetic energy of strong vortices is displayed in Figure 5 for both the infinite and finite reservoir models, showing that the thermostat drives

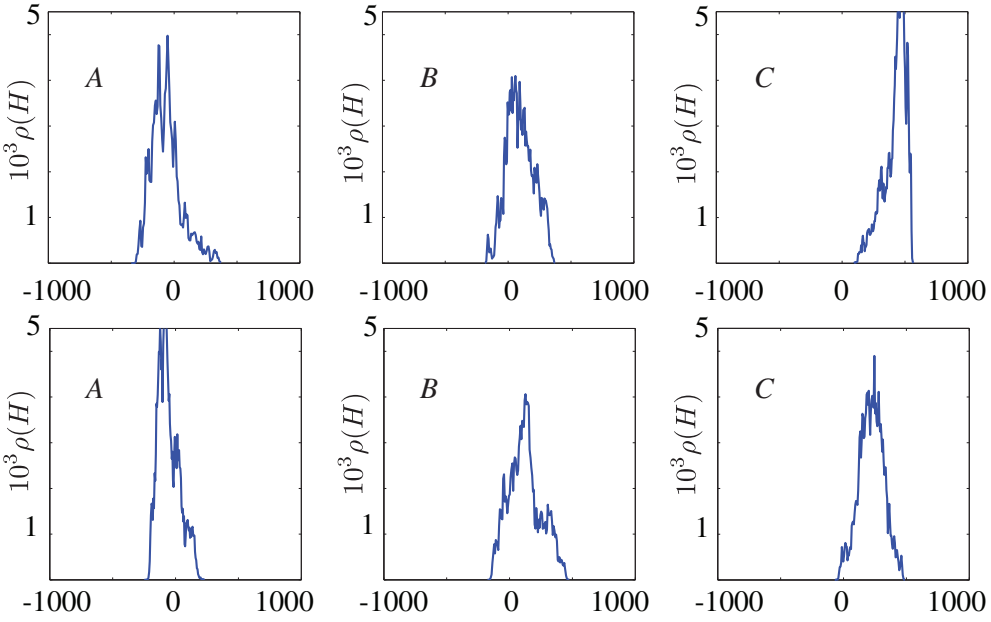

FIG. 6. *Distribution of energy for positive (A), neutral (B), and negative (C) inverse temperature states. Top: Infinite reservoir size. Bottom: Finite reservoir size.*

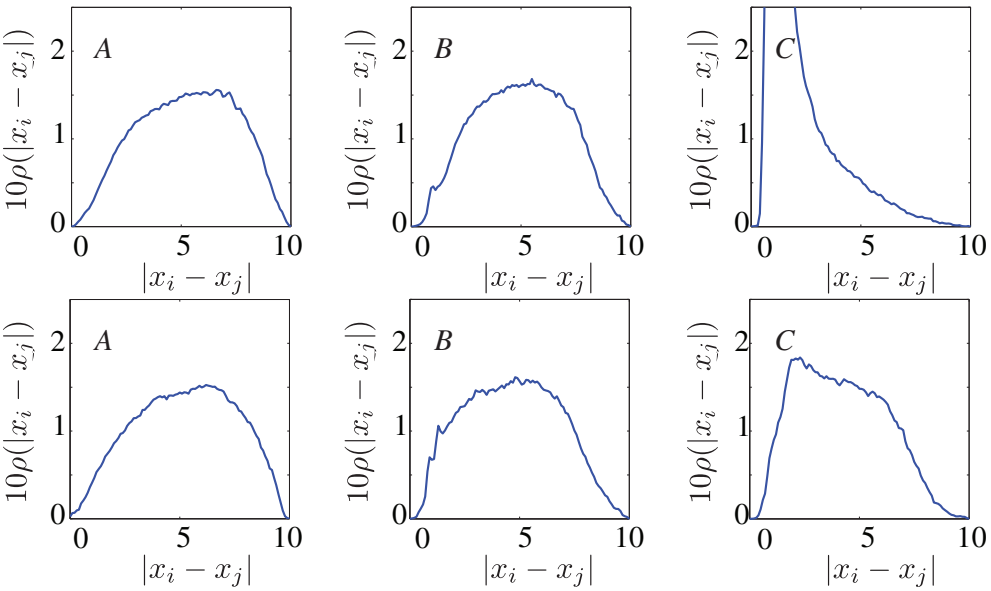

FIG. 7. *Interparticle spacing among same-signed vortices for positive (A), neutral (B), and negative (C) inverse temperature states. Top: Infinite reservoir size. Bottom: Finite reservoir size.*

the energy evolution towards the desired temperature. Figure 6 shows the probability distributions of the kinetic energy of the vortices. For the finite reservoir thermostat, the means and variances are similar to those of [2].

Figure 7 displays the histogram of distances $|x_i - x_j|$ between like-signed vortices. Bias in favor of small separations is evident at negative temperatures, consistent

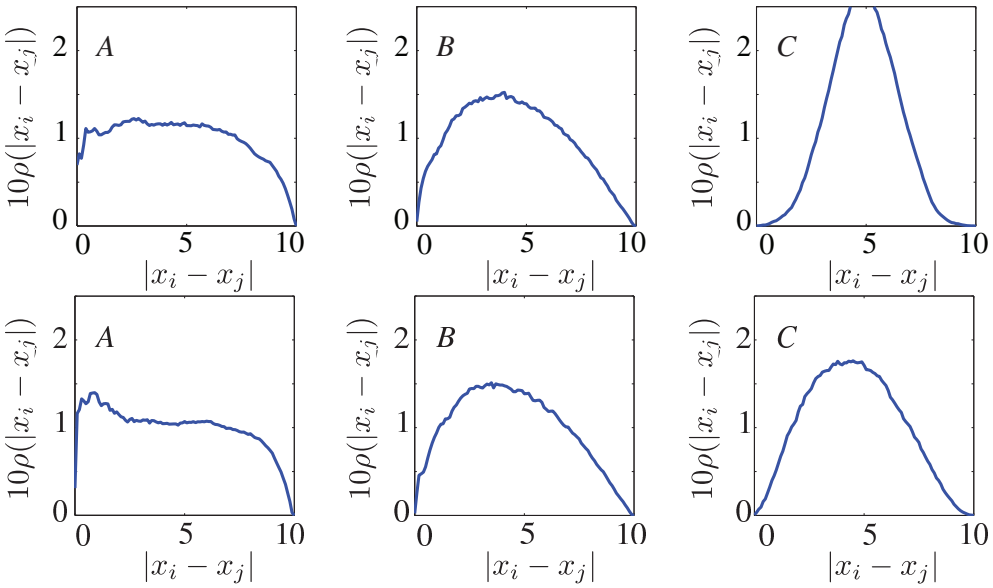

FIG. 8. *Interparticle spacing among opposite-signed vortices for positive (A), neutral (B), and negative (C) inverse temperature states. Top: Infinite reservoir size. Bottom: Finite reservoir size.*

with Onsager's predictions. The distributions are very similar to those obtained by Bühler [2]. For the infinite reservoir model, there is a large peak in the distribution at $|x_i - x_j| \approx 1$, which is inconsistent with Bühler's simulations. This occurs because too much energy is drawn from the reservoir. The comparison is recovered in the finite reservoir model.

Figure 8 shows the histograms of the distance between opposite-signed vortices. In this case, there is a somewhat milder bias towards close approaches at negative temperatures, in keeping with Onsager's ideas. The bias is less pronounced because the close approaches between a point vortex and its opposite-signed image across the domain boundary are not included in this statistic. Again the histograms are in excellent agreement with the simulation data of [2] for the finite reservoir simulation. For an infinite reservoir, the positive temperature histogram is more peaked.

Figure 9 shows histograms of the vortex distance from the origin. For positive temperature, the vortices accumulate near the wall. The finite reservoir figures are in excellent agreement with those of [2]. For the infinite reservoir, the peak at $|x_i| \approx 4.9$ is closer to the wall than for the finite reservoir, indicating that more energy is drawn from the reservoir in this case. At negative temperature, the vortices avoid the wall with high probability.

To observe the effects of temperature on a larger collection of vortices, we also simulated a set with $N = 12$, under the same conditions as above at the extremal temperatures $\beta = -0.006$ and $\beta = 0.01$. The initial positions in both cases were defined as shown in Figure 10 in the left panel. The middle and right panels of Figure 10 show characteristic snapshots for each case. Animations available from the second author's web page illustrate the dynamics for positive (http://homepages.cwi.nl/~jason/Articles/anim1.avi) and negative (http://homepages.cwi.nl/~jason/Articles/anim2.avi) temperature regimes on a short interval $t \in [1500, 1500.1]$. At positive temperatures, vortices cluster in dipoles, or translate parallel to the boundary of the domain. Because dipoles translate normal to the dipole axis until they collide with

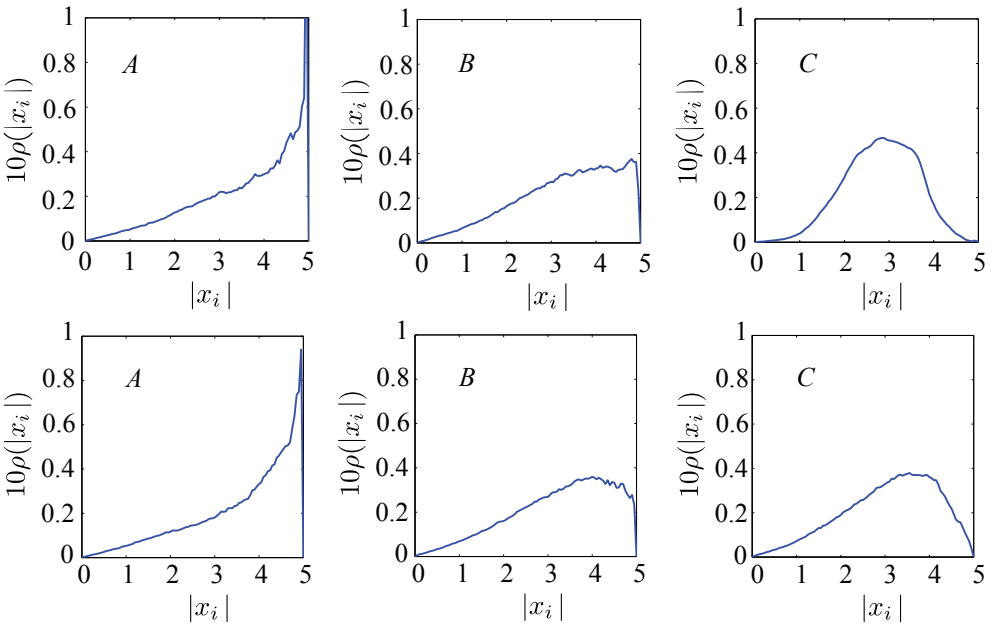

FIG. 9. *Distribution of distance from origin for positive (A), neutral (B), and negative (C) inverse temperature states. Top: Infinite reservoir size. Bottom: Finite reservoir size.*

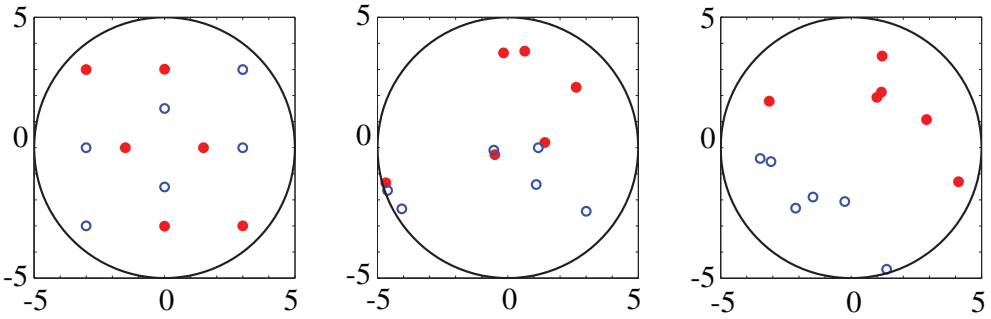

FIG. 10. *Snapshots of the case $N = 12$: The initial vortex placement (left), $\beta = 0.01$ (middle), and $\beta = -0.006$ (right). Solid (resp., unfilled) circles indicate negative (resp., positive) circulation. For positive temperature, clustering occurs pairwise; for negative temperature, large counterrotating regions occur.*

another vortex or the boundary, these pairs are short-lived. In contrast, for negative temperatures the vortices separate into two relatively stable regions of positive and negative circulation. Figure 11 shows a snapshot of the stream function from the positive and negative temperature simulations. For negative temperatures the vorticity is more concentrated in two counterrotating patches.

6. Conclusions. In this paper we provide proof of concept that the energy exchange between a set of strong point vortices and a reservoir of unresolved weak point vortices can be well modelled with a simple thermostat device that adds only a single degree of freedom to the phase space of the large-scale flow. Specifically, we are able to recover the canonical statistics of the strong vortices, as obtained from direct numerical simulations in [2]. By constructing a thermostat for general energy-dependent equilibrium distributions, we model a canonical ensemble with a finite reservoir.

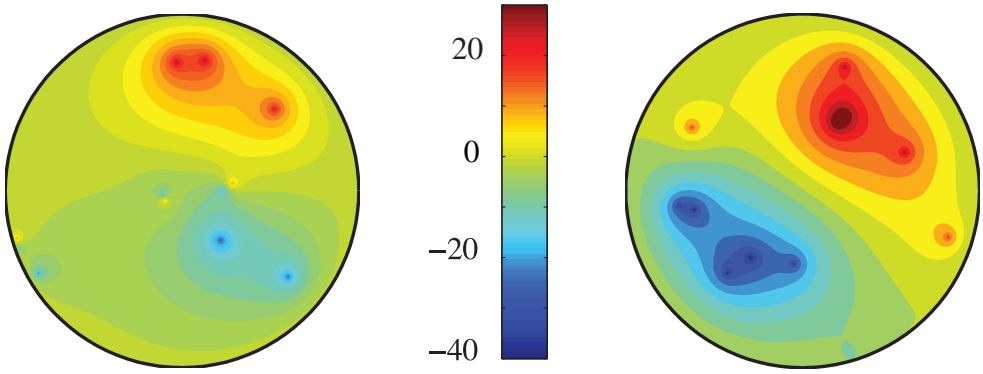

FIG. 11. *Snapshots of the stream function for case $N = 12$, $\beta = 0.01$ (left), and $\beta = -0.006$ (right). For negative temperature, clustering of like-signed vortices yields two strong counterrotating vortices. See animations at the second author's web page http://homepages.cwi.nl/∼jason/Articles/anim1.avi ($\beta = 0.01$) and http://homepages.cwi.nl/∼jason/Articles/anim2.avi ($\beta = 0.006$).*

Acknowledgment. We express thanks to Jacques Vanneste for fruitful discussions during the early stages of this work.

REFERENCES

[1] S. D. BOND, B. J. LEIMKUHLER, AND B. B. LAIRD, *The Nosé-Poincaré method for constant temperature molecular dynamics*, J. Comput. Phys., 151 (1999), pp. 114–134.
[2] O. BÜHLER, *Statistical mechanics of strong and weak point vortices in a cylinder*, Phys. Fluids, 14 (2002), pp. 2139–2149.
[3] A. BULGAC AND D. KUSNEZOV, *Canonical ensemble averages from pseudomicrocanonical dynamics*, Phys. Rev. A, 42 (1990), pp. 5045–5048.
[4] A. J. CHORIN, *Vorticity and Turbulence*, Appl. Math. Sci. 103, Springer-Verlag, New York, 1994.
[5] A. J. CHORIN, O. H. HALD, AND R. KUPFERMAN, *Optimal prediction and the Mori-Zwanzig representation of irreversible processes*, Proc. Natl. Acad. Sci. USA, 97 (2000), pp. 2968–2973.
[6] G.-H. COTTET AND P. D. KOUMOUTSAKOS, *Vortex Methods. Theory and Practice*, Cambridge University Press, Cambridge, UK, 2000.
[7] D. R. DURRAN, *Numerical Methods for Wave Equations in Geophysical Fluid Dynamics*, Texts Appl. Math. 32, Springer-Verlag, New York, 1999.
[8] G. GALLAVOTTI, *Dynamical ensembles equivalence in fluid mechanics*, Phys. D, 105 (1997), pp. 163–184.
[9] W. G. HOOVER, *Canonical dynamics: Equilibrium phase-space distributions*, Phys. Rev. A, 31 (1985), pp. 1695–1697.
[10] W. HUNDSDORFER AND J. VERWER, *Numerical Solution of Time-Dependent Advection-Diffusion-Reaction Equations*, Springer Ser. Comput. Math. 33, Springer-Verlag, Berlin, 2003.
[11] A. KHINCHIN, *Mathematical Foundations of Statistical Mechanics*, Dover, New York, 1960.
[12] B. LEIMKUHLER, *Generalized Bulgac-Kusnezov methods for sampling of the Gibbs-Boltzmann measure*, Phys. Rev. E, 81 (2010), 026703.
[13] B. LEIMKUHLER, E. NOORIZADEH, AND F. THEIL, *A gentle stochastic thermostat for molecular dynamics*, J. Stat. Phys., 135 (2009), pp. 261–277.
[14] C. LIM AND J. NEBUS, *Vorticity, Statistical Mechanics, and Monte Carlo Simulation*, Springer Monogr. Math., Springer-Verlag, New York, 2007.
[15] A. J. MAJDA AND A. L. BERTOZZI, *Vorticity and Incompressible Flow*, Cambridge Texts Appl. Math. 27, Cambridge University Press, Cambridge, UK, 2002.
[16] A. J. MAJDA AND X. WANG, *Non-linear Dynamics and Statistical Theories for Basic Geophysical Flows*, Cambridge University Press, Cambridge, UK, 2006.

[17] J. Mattingly, A. M. Stuart, and D. J. Higham, *Ergodicity for SDEs and approximations: Locally Lipschitz vector fields and degenerate noise*, Stochastic Process. Appl., 101 (2002), pp. 185–232.
[18] J. H. Mentink, M. V. Tretyakov, A. Fasolino, M. I. Katsnelson, and Th. Rasing, *Stable and fast semi-implicit integration of the stochastic Landau–Lifshitz equation*, J. Phys.: Condens. Matter, 22 (2010), 176001.
[19] S. Nosé, *A molecular dynamics method for simulations in the canonical ensemble*, Mol. Phys., 52 (1984), pp. 255–268.
[20] S. Nosé, *A unified formulation of the constant temperature molecular dynamics methods*, J. Chem. Phys., 81 (1984), pp. 511–519.
[21] M. Oliver and O. Bühler, *Transparent boundary conditions as dissipative subgrid closures for the spectral representation of scalar advection by shear flows*, J. Math. Phys., 48 (2007), 065502.
[22] L. Onsager, *Statistical hydrodynamics*, Nuovo Cimento (9), 6 (1949), pp. 279–287.
[23] G. A. Pavliotis and A. M. Stuart, *Multiscale Methods: Averaging and Homogenization*, Springer-Verlag, New York, 2008.
[24] R. Salmon, *Lectures on Geophysical Fluid Dynamics*, Oxford University Press, New York, 1998.
[25] J. B. Weiss and J. C. McWilliams, *Nonergodicity of point vortices*, Phys. Fluids A, 3 (1991), pp. 835–844.